JOURNAL OF MATERIALS SCIENCE 3 (1968) 191–205

Effect of Microstructure on Superconducting Properties of Mo/34 at.% Re Alloy

M. J. WITCOMB, A. ECHARRI, A. V. NARLIKAR, D. DEW-HUGHES
Department of Physics, The University, Lancaster, UK

Received 30 October 1967, and in revised form 8 December

The effect of deformation and heat-treatments on magnetisation of superconducting Mo/34 at. % Re alloy was investigated. The microstructure was studied using optical and electron microscopy. The values of the parameter κ of the GLAG theory were determined by using three different methods, and they are found to be in accordance with some of the predictions of the Maki theory. The results show that in deformed specimens the magnetic hysteresis is mainly due to the interaction of Abrikosov supercurrent vortices with dislocation tangles; both twin boundaries and grain boundaries are relatively ineffective in causing flux hindrance. The hysteresis observed after annealing has been explained in terms of the occurrence of dislocation rearrangement and the precipitation of the sigma phase. Flux-pinning by dislocation tangles has been treated as a special case of pinning by normal particles and a magnitude of the resulting pinning force is obtained. The experimental results are compared with the predictions of a theoretical model of flux-pinning.

1. Introduction

It is now well established that the irreversible magnetic properties and current carrying capacity of hard or type II superconductors are largely governed by the interaction of Abrikosov's supercurrent vortices with microstructural defects. Superconducting materials suitable for most commercial and technological applications are those which meet with three requirements (i) high critical temperature and high upper critical field; (ii) large current carrying capacity; (iii) good workability. Few materials satisfy all of these requirements and in general materials having the desired superconducting properties are poor in workability. However, certain alloys of Mo and Re form an exception to this and are consequently of particular interest.

Superconducting properties of Mo/Re alloys have not been studied as extensively as those of pure Nb and some of its alloys. In 1955 Hulm [1] noted certain Mo/Re alloys to have a high critical temperature. The subsequent work of Blaugher *et al* [2] showed that in Mo-rich alloys, the critical temperature increases with the Re content, and reaches a maximum at 12.25° K for Mo/38 at. % Re. The work of Kunzler and his co-workers [3] demonstrated that the cold-worked Mo/25 at. % Re alloy could be used in solenoids to generate magnetic fields of 15.5 kOe at 1.5° K. More recently, the thermal, electrical, and magnetic properties of Mo/(32-35) at. % Re alloys have been studied by Lerner *et al* [4, 5] who found that some of these properties are influenced by the presence of the sigma phase. The maximum workability of the alloy is known to occur with a composition of about 35 at. % Re [6]. The phase diagram of Mo/Re system is well known [7]. The 34 at. % Re alloy studied in this investigation lies in the two-phase region, consisting of a BCC solid solution (superconducting at 4.2°) and the tetragonal sigma phase (non-superconducting). The size and distribution of the sigma phase precipitates are largely governed by the precise heat treatments [8] and they have been studied recently using transmission electron microscopy [9]. The normal precipitates in type II superconductors are known to interact

strongly with supercurrent vortices [10]. The pinning of flux by normal particles has been studied both experimentally and theoretically and the strength of the interaction is found to depend upon the size and distribution of the precipitates in the material [11].

The effect of deformation on superconducting properties has been studied by several workers, and it is found that the current-carrying capacity and the magnetic hysteresis of the specimen are enhanced by cold-work [12, 13]. More recently, the effect of deformation on the microstructure and superconducting properties of Nb and Nb-alloys has been reported [14], and it is found that in these materials dislocation tangles produced by deformation are chiefly responsible for flux-pinning. The Mo/Re differs from the Nb-alloys in that, when deformed at room temperature, it undergoes profuse twinning. The critical stress for twinning in Mo is markedly lowered by Re addition. The twin boundaries in the deformed alloy have been studied recently by a number of workers using transmission electron microscopy [15-18]. It has been generally observed that the materials which twin easily when lightly deformed show, in contrast to Nb and Nb-alloys, little sign of dislocation tangling and the familiar cell structure [19].

Type II superconductors have been thoroughly discussed in recent review articles [20-23]. The phenomenological theory of Ginzburg and Landau, valid near the critical temperature T_c, introduces a dimensionless parameter κ, given by

$$\kappa_{GL} = 2^{\frac{1}{2}} \frac{e^* H_c}{\hbar c} \lambda^2_L \qquad (1)$$

where λ_L is the London penetration depth, and e^* the effective charge on the basic superconducting particle, an electron pair ($e^* = 2e$). The subsequent work of Abrikosov and Gor'kov, essentially based on the Ginzburg-Landau theory, showed that κ for type II superconductors could be expressed in terms of H_c, H_{c_1} and H_{c_2}. as follows

$$\kappa_1 = H_{c_2}/\sqrt{2}\, H_c \text{ [24]} \qquad (2)$$

$$\kappa_2 = f\left(\frac{dM}{dH}\right) \text{ [24]} \qquad (3)$$

$$\kappa_3 = f\left(\frac{H_{c_1}}{H_c}\right) \text{ [25]} \qquad (4)$$

where $\kappa_1 = \kappa_2 = \kappa_3 = \kappa_{GL}$ only very near T_c. Recently, the Ginzburg-Landau theory has been extended for temperatures $T \ll T_c$, and it is found that the value of κ_1 at $T = 0$ is 20% [26] or 25% [27] higher than the one given by equation 2 near T_c. For pure metals (the normal electron mean free path l very large) the theory predicts [26, 28] the variation of κ_2 with temperature ($T \ll T_c$) to be very close to that of κ_1; both κ_1 and κ_2 increasing together with decreasing temperature. For alloys (l small), on the other hand, the theory finds [26, 28] for $0 < T < T_c$, $\kappa_2 \ll \kappa_1$, and for certain alloys, depending on the value of l, the theory predicts κ_2, in contrast to κ_1, to decrease with decreasing temperature [26]. For alloys, the theory [26] suggests that the value of κ_3 at $T = 0$ should be 53% higher than calculated by equation 4 at $T = T_c$. The above conclusions of the Maki theory are summarised in fig. 1. Consequently, for the Mo/34% Re alloy it is expected that the values of κ_1, κ_2 and κ_3 measured at 4.2° K ($T_c \gg 4.2°$) will, in general, not be the same.

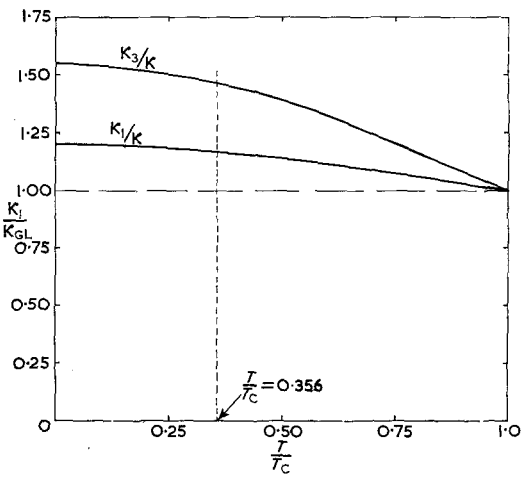

Figure 1 Theoretical variation of κ_1 and κ_3 with temperature (after Maki [26]).

The present investigation was carried out to check some of the above predictions of the Maki theory, and to study the effect of microstructure on the superconducting properties of the Mo/34% Re alloy.

2. Experimental

The Mo/34 at. % Re alloy was supplied by Engelhard Industries Limited, Sutton, Surrey. It was of commercial purity and in the form of a thin sheet of thickness 0.25 mm. Thin foils for transmission electron microscopic examination were prepared by electro-polishing the specimen in a bath of concentrated sulphuric acid. The

polishing was done at room temperature with a current density of 1 A/cm^2 at 15 V. All the specimens were examined in a Siemens Elmiskop 1 A microscope operating at 100 kV. For the optical examination, the specimens were first polished as above, and subsequently etched in a bath of 2:2:1 mixture of nitric, sulphuric and hydrofluoric acids.

All superconducting measurements were made at 4.2° K. The samples for the magnetisation measurements were in the form of cold-rolled strips measuring 10 × 1 × 0.25 mm. The magnetisation of the specimen was measured using the conventional ballistic galvanometer method reported earlier [14]. The magnetic field was generated by a superconducting solenoid wound from Nb/25% Zr alloy wire, which was capable of producing fields up to 30 kOe.

It has been found that the critical current curves (J_c/H) of specimens deformed by rolling are considerably different when measured along and perpendicular to the rolling plane [53, 54]. Also, the microstructure seen along and transverse to the rolling plane is found to be different [54-56]. The anisotropy effects in magnetisation measurements have not been explored yet, but there is very little doubt that the magnetisation of a rolled strip measured with the applied field along the perpendicular to the rolling plane will be different. In this investigation all magnetisation measurements were made with the applied magnetic field parallel to the rolling plane and to the rolling direction and the microstructure observed was as seen in this plane.

The normal-state resistivity measurements, at both room temperature and at 4.2° K, were made by using a four-probe technique. The resistivity at 4.2° K was measured by placing the specimen carrying a steady current at the centre of the magnet situated inside a liquid helium cryostat. The magnetic field was gradually increased and the voltage across the specimen was measured when the magnetic field was sufficiently high to completely quench the superconductivity of the specimen. The procedure was repeated outside the cryostat for the measurement of room temperature resistivity.

3. Microstructure

3.1. As-Received Material

Optical examination of an etched sample showed the grain-boundary structure typical of a recrystallised material. Grain size varied considerably within the specimen; the mean grain diameter was 0.06 mm. The grains were, in general, free of defects, although occasional twin boundaries were observed in some specimens. Transmission electron microscope examination revealed most of the regions of the specimen to be free of dislocations. Some specimens contained a few, isolated, long dislocations. These dislocations and twins may have been originally present in the material or they may have been introduced during handling of the specimen. No precipitates, sigma-phase or other, were observed. From these observations it is concluded that the as-received material had been well-annealed in a temperature range which did not allow of sigma-phase precipitation.

3.2. Deformed Specimens

The as-received specimen was deformed by varying amounts, by cold-rolling, and the resulting microstructure was examined using optical and electron microscopy. After 3% deformation the optical examination revealed a high density of twins; almost every grain contained one or more twin lamellae (fig. 2). The increase in deformation seemed to have very little effect on the density of twins; the width of the twin bands, however, increased with strain. Table I gives the measured values of twin widths and densities in the specimens deformed to different strains. An estimate of twin-density was obtained by counting the number of intersections per mm made by the twin bands with a set of random lines drawn on the micrograph. The figures given in table I are the average values as obtained from at least four different micrographs. Similar observations were made on this alloy by Reid *et al* [29] who found that the twins increase in number only at small strains, but thereafter their width increases slowly with further deformation. Geil and Carwile's studies on α-iron [30] support the above contention. The twin boundaries at low strains were, in general, straight and parallel sided. At higher deformations, however, they became fragmented and notches were seen on them (fig. 3). It has been suggested that the notches result when the stresses associated with a twin are relieved by slip [31]. The observed interruptions in twin boundaries are believed to be due to the dislocation tangles causing hindrance to twin growth [16]. An array of dislocations passing through a twin lamella can also lead to a reduction in the thickness of the twin, or even its complete local annihilation [16].

The crystallography of twins in Mo/Re alloys,

TABLE I

Specimen	As-received	3% Deformed	9% Deformed	16% Deformed	21% Deformed	26% Deformed	37% Deformed
Lineal density of twins, N_L (intersections per mm)	Nil	37	37	38	38	38	38
Twin width (microns)	Nil	3.0	5.6	7.3	8.2	9.0	9.8

produced after room temperature deformation, has been extensively studied by several workers and it is found that the twinning occurs on $<111>$ $\{112\}$ shear systems [16-19]. The twin-growth in BCC metals is conveniently described by the movement of a set of $a/6$ $<111>$ partial dislocations in successive $\{112\}$ planes. This has been confirmed by direct observation by transmission electron microscopy [18]. Several mechanisms have been proposed to explain how the dissociation and the movement of the dislocations take place and these have been reviewed recently [19]. In this investigation no attempt was made to decide between these models.

The dislocation structure in deformed specimens as revealed by electron microscopy had two distinct features: (i) dislocations of ordinary slip type, i.e. produced by the slip of the bulk specimen, (ii) a dislocation structure which was directly related to deformation twinning. Pre-existing twins do not provide a strong barrier to slip dislocations but they can provide an extremely strong barrier to the growing twins [32]. Deformation twins are associated with large internal strains, and for a growing twin the stress concentration is considerable at its tip [33]. Sleeswyk [33] suggested that the stress at the tip is relieved by the creation ahead of the twin boundary of "emissary dislocations", formed by dissociation of a twinning dislocation by the reaction

$$a/6\,[1\,1\,1] \rightarrow a/3\,[\bar{1}\,\bar{1}\,\bar{1}] + a/2\,[1\,1\,1].$$

The subsequent work of Votava and Sleeswyk [16] confirmed the existence of emissary dislocations in Mo/Re alloys. Such emissary dislocations were also observed in the present investigation during early stages of deformation. A second kind of dislocation structure associated with twins was observed at the twin interface. Hull [34] has explained the formation of slip dislocations at the interface by a mechanism involving coalescence by cross-slip of three twinning screw dislocations on the adjacent parallel $\{1\,1\,2\}$ planes; the dislocation reaction is

$$a/6\,[1\,1\,1] + a/6\,[1\,1\,1] + a/6\,[1\,1\,1] \rightarrow a/2\,[1\,1\,1].$$

This reaction leads to an increase in energy, but it may occur under the action of a high shear stress produced by a big pile-up of twinning dislocations.

Fig. 4 shows the dislocation structure observed in the specimen deformed by 2%. The dislocations seen are of ordinary slip type. Also seen are a large number of elongated dislocation loops which are believed to be generated by a mechanism involving double cross slip of screw dislocations containing jogs [35]. Cusps can be seen in many of the dislocations, and the actual pinching-off of the dislocation jog to form an elongated dislocation loop is apparent at A. The traces of long dislocations are believed to be those present prior to deformation. They are not seen distinctly because the orientation of the specimen foil is not favourable for them for optimum diffraction contrast. The emissary type and the interface dislocations were also observed in the specimen as mentioned above, but they were present in the different region of the foil and are not seen in fig. 4. The dislocation structure observed after 4 and 8% deformations is shown in figs. 5 and 6. The dislocation density was considerably increased, and it was no longer possible to identify the emissary and the ordinary slip dislocations separately. Also seen in figs. 5 and 6 is the apparent increase in the density of dislocation loops as a result of deformation. The dislocation distribution in the 4% deformed specimen was in general quite uniform, but after 8% deformation some evidence of tangling of dislocations was noticed. In the 12% deformed specimen (fig. 7) the tangles had joined-up to form the familiar cell structure. After 16% deformation the specimen showed a well developed cell structure, fig. 8. The cell walls were mainly found to be along $<111>$ direction and this is the direction in which the emissary dislocations lie. A specimen deformed to 24% strain showed an increase in dislocation density.

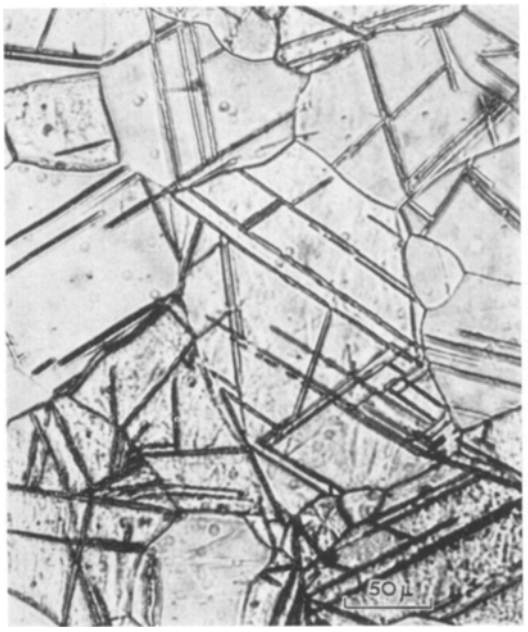

Figure 2 Optical micrograph of Mo/Re alloy after 3% deformation showing twins.

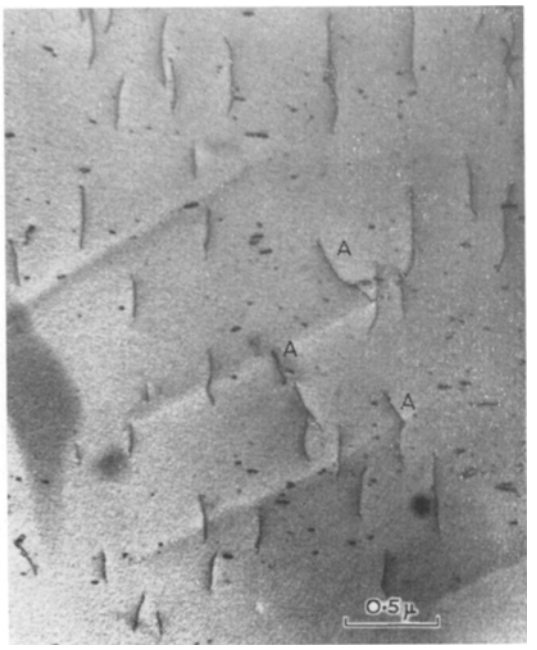

Figure 4 Electron micrograph of Mo/Re alloy after 2% deformation showing pinched off dislocation loops. Note the cusps at A.

Figure 3 Optical micrograph of Mo/Re alloy after 27% deformation showing notched twins.

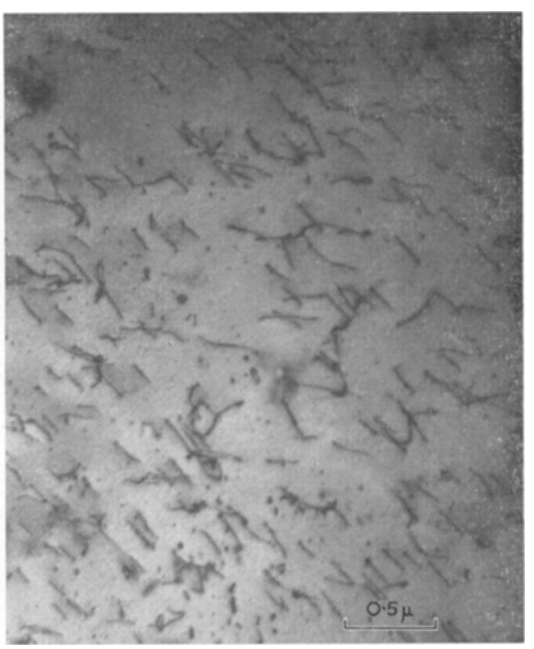

Figure 5 Electron micrograph after 4% deformation.

The loops were essentially in the tangles of the cell walls, and in this specimen it was not possible to estimate their densities. Using the method suggested by Ham [36] and taking average thick-

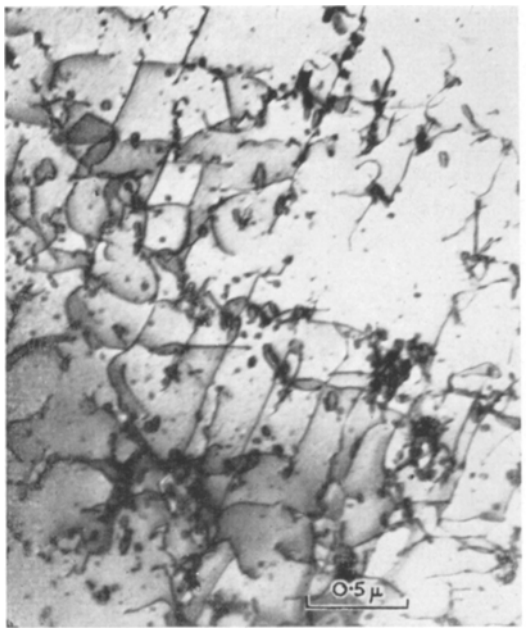

Figure 6 Electron micrograph after 8% deformation. Note beginning of cell structure.

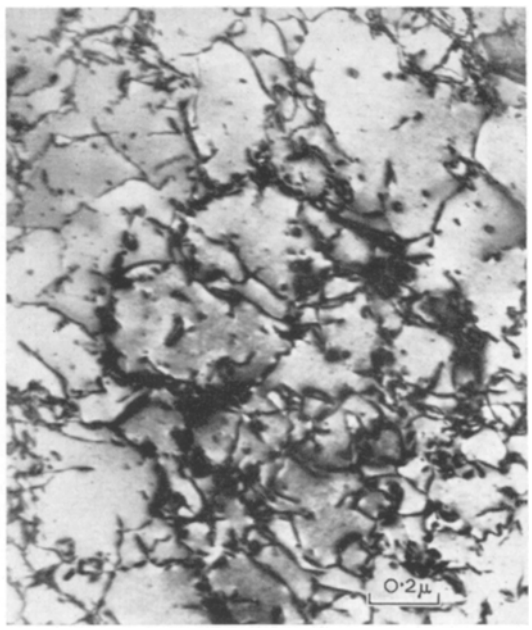

Figure 7 Electron micrograph after 12% deformation. Cells are now seen quite clearly.

ness of the foil as 2500 Å, the measured values of dislocation densities in deformed specimens are given in table II.

Figures shown in the table are the average values as obtained from at least four different micrographs. The dislocation cells produced after deformation were irregular in both size and shape and it was found that the mean value of the cell size, i.e. the distance between the cell walls, L, was roughly invariant under deformation. The width of the cell walls, d, on the other hand, increased with deformation (table II). These results are entirely consistent with those reported earlier on Nb and Nb-alloys [14]. Since a review of deformation structure in BCC metals has already been made [14], no further attempt will be made to describe the cell formation in this paper.

The effect of deformation on grain size was measured. The specimens deformed up to 37% by rolling showed hardly any decrease in the grain size. The grain size varied considerably within the specimen, but its mean value remained unaltered after deformation. In this investigation

TABLE II

Specimen	As-received	2% Deformed	4% Deformed	8% Deformed	12% Deformed	16% Deformed	24% Deformed
Average dislocation density per cm²	8×10^8	1.9×10^9	4.8×10^9	1.4×10^{10}	1.8×10^{10}	2×10^{10}	2.3×10^{10}
Dislocation density in tangles, per cm²	—	—	—	—	2.8×10^{10}	3.1×10^{10}	3.7×10^{10}
Density of dislocation—loops, per cm³	—	6.0×10^4	9.3×10^4	2.2×10^5	—	3.5×10^5	—
Mean distance between cell walls, L (microns)	—	—	—	—	0.35	0.35	0.35
Average width of the cell wall, d (microns)	—	—	—	—	0.03	0.06	0.09

the effect of higher deformations on the grain size was not studied.

3.3. Heat-Treated Specimens

The specimens deformed to 16% strain were annealed for 1 h in an argon atmosphere at temperatures of 850, 950, 1050, and 1200° C. Transmission electron microscopy of the specimen annealed at 850° C showed the occurrence of dislocation rearrangement. Dislocations within the cells had moved into the walls making them more dense and well defined. The dislocation structure observed after annealing at 950° C was essentially very similar to the above. This specimen, in addition, also showed regions where dislocations had interacted to form the polygonised sub-grain boundaries consisting mainly of the hexagonal networks of dislocations formed by the reaction

$$a/2\,[1\,1\,1] + a/2\,[\bar{1}\,1\,\bar{1}] \rightarrow a\,[0\,1\,0]$$

The microstructure observed in the specimen annealed at 1050° C was a heavily polygonised one consisting of pure twist and tilt boundaries, and is shown in fig. 9.

None of the specimens annealed at 850, 950 and 1050° C showed any precipitates.

The specimen annealed for 1 h at 1200° C, and cooled slowly inside the furnace, showed a presence of precipitates (fig. 10) which, by means of the selected area diffraction technique, could

Figure 8 16% deformation. Cell structure is now completely formed.

Figure 9 16% deformed and annealed 1 h at 1050° C. Note polygonised cell structure.

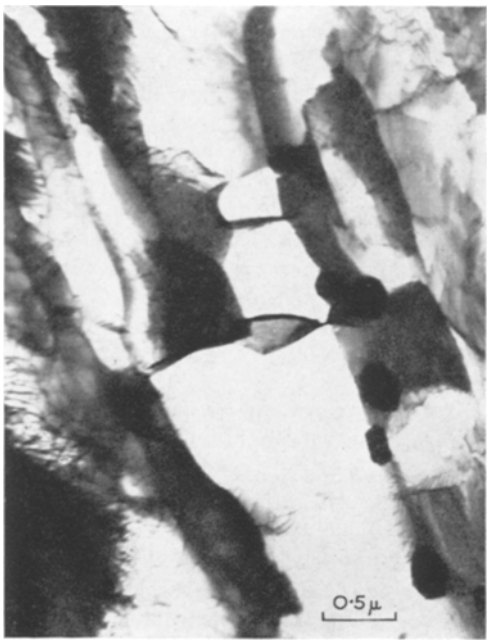

Figure 10 16% deformed and annealed 1 h at 1200° C, showing precipitates of sigma-phase.

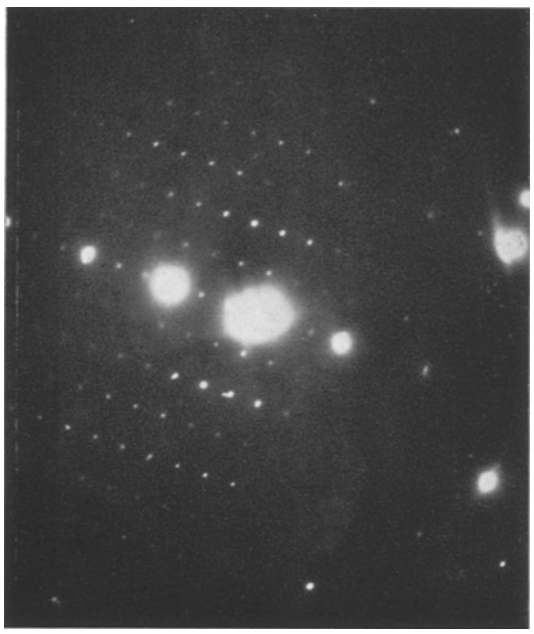

Figure 11 Selected area diffraction photograph for sigma-precipitate.

easily be identified as the precipitates of the tetragonal sigma-phase. A typical diffraction pattern obtained from one such precipitate is shown in fig. 11; the intense spots correspond to the matrix, while the closely spaced weaker ones correspond to the precipitates. No precipitates of sigma-phase were observed after annealing the specimen below 1150° C. This agrees with the work of Knapton [37] who found that the sigma-phase in the Mo/Re system is stable only at temperatures of 1150° C and above. Raising the annealing temperature to 1300° C produced larger precipitates.

4. Superconducting Properties

4.1. As-Received Specimen

Magnetisation of the as-received material exhibited very little hysteresis and is shown in fig. 12. The curve is completely reversible at high fields, but becomes gradually irreversible as the magnetic field is lowered. Due to lack of experimental facilities, the specimen could not be annealed at a sufficiently high temperature ($T > 1800°$ C) to obtain a more reversible magnetisation curve. It has been suggested that in perfectly homogeneous material there will be some irreversibility due to surface currents, which are diminished if the specimen is coated with a layer of normal metal [38]. The magnetisation curves of samples coated with copper or aluminium were, however, almost identical with that for the as-received material.

For an irreversible specimen H_{c_1} is, in general, difficult to determine. However, two methods have been suggested recently and have been successfully used for Zr/V alloys [39]. In one method, magnetisation of the specimen in the Meissner region is carefully measured, and the field at which the deviation from the linearity of the Meissner region ($H = -4\pi M$) begins is carefully determined; this field is taken as H_{c_1}. The other method involves the accurate measurement of the remanent induction within the sample [40]. In the case of Zr/V alloys both techniques are found to give consistent values of H_{c_1} [39]. In the present investigation, only the first of the above two methods was used in determination of H_{c_1} for the as-received specimen, and the value thus obtained was 368 Oe. A fully reversible magnetisation curve was estimated by extrapolating the reversible portion of the curve for the as-received material at high fields back to this value of H_{c_1}. This curve is shown in fig. 12.

Using the reversible curve of fig. 12, κ_1, κ_2, and κ_3 were determined from equations 2, 3 and 4.

(i) κ_1 The magnetisation curve of the as-received specimen gives H_{c_2} as 11340 Oe. The thermodynamic critical field H_c at 4.2° K, as measured from the area of the reversible magnetisation curve, is found to be 1460 Oe. Taking γ (electronic specific heat coefficient) for Mo/34 % Re alloy as 4110 erg/cm^3 (° K)^2 [41] and $T_c = 11.8°$ K [2], Mühlschlegel's calculations [42], based on the BCS theory, yield H_c (4.2° K) = 1580 Oe. The Gorter-Casimir model [43], on the other hand, gives H_c(4.2° K) = 1620 Oe. The validity of both BCS and Gorter-Casimir theories to type II alloys is open to criticism, and it is not entirely unexpected that the calculated values of H_c are about 10% higher than the experimental value.

Equation 2 gives,

$$\kappa_1 = \frac{H_{c_2}}{\sqrt{2}\, H_c} = 5.5$$

(ii) κ_2 Equation 3 is written as

$$\left(\frac{dM}{dH}\right)_{H_{c_2}} = [1.16(4\pi)\,(2\kappa_2^2 - 1)]^{-1}$$

This gives $\kappa_2 = 5.2$

(iii) κ_3 $f(H_{c1}/H_c)$ has been evaluated numerically by Harden and Arp [25]. Taking H_{c_1} as found above, and H_c from the area of the reversible curve, $\kappa_3 = 6.9$.

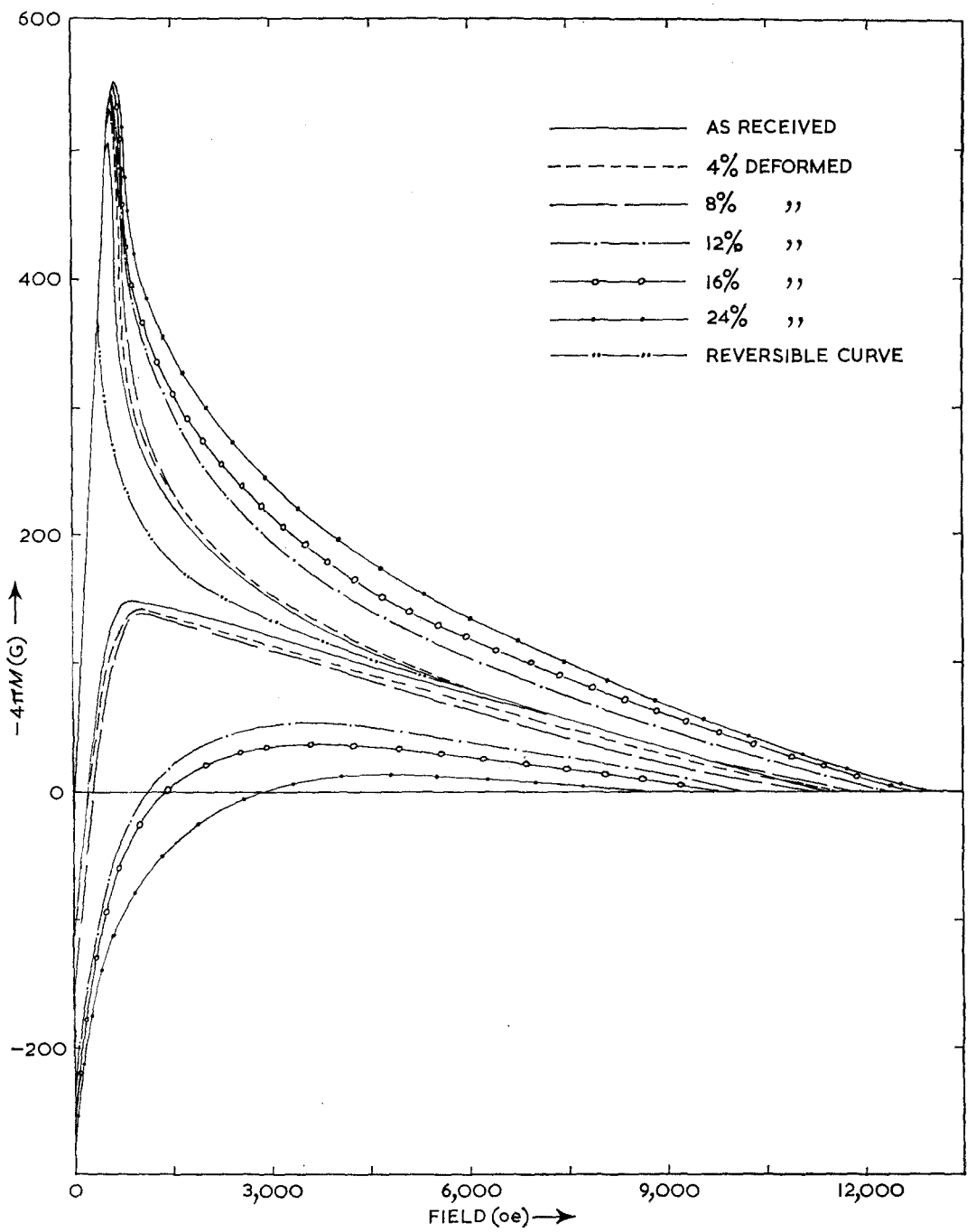

Figure 12 Magnetisation curves for deformed Mo/Re specimens. $+4\pi M$ values near H_{c_2} (H decreasing) for all the curves, were very close to the H axis, and they are omitted from the figure for the sake of clarity.

The three values of the parameter κ obtained are different, as predicted by the Maki theory, and $\kappa_1 > \kappa_2$, in accordance with the theory for alloys.

To compare these results quantitatively with the Maki theory, for Mo/34% Re, $T_c = 11.8°$ K; from fig. 1 at 4.2° K ($T/T_c = 0.356$),

$$\kappa_1/\kappa_{GL} = 1.16$$

and

$$\kappa_3/\kappa_{GL} = 1.46$$

κ_{GL} is not known. But if the Maki theory is correct, at $T/T_c \simeq 0.356$

$$\kappa_3/\kappa_1 \text{ (theory)} = 1.46/1.16 \simeq 1.26$$

The experimental values of κ_1 and κ_3 give κ_3/κ_1 (experimental) $\simeq 1.26$. These results at 4.2° K are, quantitatively in good agreement with the predictions of the Maki theory. Currently experiments are in progress to check these results more extensively at lower temperatures; these will be reported elsewhere.

4.2. Deformed Material

The effect of deformation on the upper critical field was carefully studied. Magnetisation measurements made earlier on Nb and Nb-alloys had revealed no observable change in the value of H_{c_2} after deformation [14]. However, the present investigation did show a noticeable increase after cold-working. Magnetisation curves of as-received specimens cold-rolled by 4, 8, 12, 16, and 24% are shown in fig. 12. The measured values of H_{c_2} at 4.2° K are tabulated in table III. Deformation is expected to have only a small effect on H_c and T_c. Assuming them to be invariant, values of κ_1 were determined using equation 2, and are given in the table. Also shown are the values of H_{c_1} as calculated from κ_1, the Maki theory (fig. 1), and Harden and Arp's computed results.

The resistivity measurements showed an increase in the normal state resistivity when the samples were deformed. Livingston [20], using Goodman's formula [44] has shown that H_{c_2} is related to normal state resistivity by a simple expression

$$(H_{c_2})_{0°\,K} = 2.58 \times 10^{-2}\, \gamma T_c\, \rho_n \qquad (5)$$

where ρ_n is the normal state resistivity in $\mu\Omega$ cm; T_c and γ are as defined in 4.1. The value of ρ_n for the as-received sample increased from 7.7 to 8.9 $\mu\Omega$ cm after it was deformed by 29%. Assuming γ and T_c as invariant under deformation, $H_{c_2}(29\%)/H_{c_2}$(as-received) $= \rho_n(29\%)/\rho_n$ (as-received) $= 1.15$. Magnetisation of the 29% deformed specimen was not investigated, and hence H_{c_2} for this sample is not known. However, the measured values of H_{c_2} for the as-received and 24% deformed specimens give $H_{c_2}(24\%)/H_{c_2}$(as-received) $= 1.14$. This is entirely consistent with the ratio obtained above using the resistivity data.

Substituting the values of γ, T_c, and ρ_n in equation 5, and making the appropriate reduction to 4.2° K, values of H_{c_2}(4.2° K) are found to be more than 25% smaller than the experimental ones. The disagreement is probably due to the fact that equation 5 is based on the assumption that κ is large (say, >10), a condition which is not fulfilled in this alloy.

The effect of deformation on H_{c_1} was not studied in the present investigation, and the calculated values of H_{c_1} of table III remain to be checked. This is currently being carried out using the remanent induction method [40] and will be reported elsewhere.

The effect of deformation on magnetisation was qualitatively very similar to that observed in Nb and Nb-alloys [14]. The magnetisation curves became more hysteretic (fig. 12), and the remanent flux increased with cold-work. The remanent flux expressed as a fraction of H_{c_2} was taken as a convenient measure of the irreversibility. This is plotted in fig. 13 against percentage deformation, taking into consideration the size effect [14].

The variation of the fraction of the remanent flux with percentage deformation is qualitatively very similar to that of pure Nb [14]. It is interesting to note that the remanent flux remains practically unaltered until the initial 4% deformation. The knee of the curve is somewhere between 12% and 15% after which the increase in hysteresis with deformation becomes less. The increase is a maximum between 4% and 12% deformation.

When the observed variation of the fraction of the remanent induction is considered along with the microstructure, it becomes evident that the interaction of flux lines with the twin boundaries must be small. Had this interaction been strong, a significant increase in magnetic hysteresis

TABLE III

Specimen	As-received	4% Deformed	8% Deformed	12% Deformed	16% Deformed	24% Deformed
H_{c_2}(Oe)	11340	11500	11700	12310	12790	12950
κ_1	5.50	5.57	5.67	5.96	6.19	6.27
H_{c_1}(Oe)	368	362	356	346	336	333

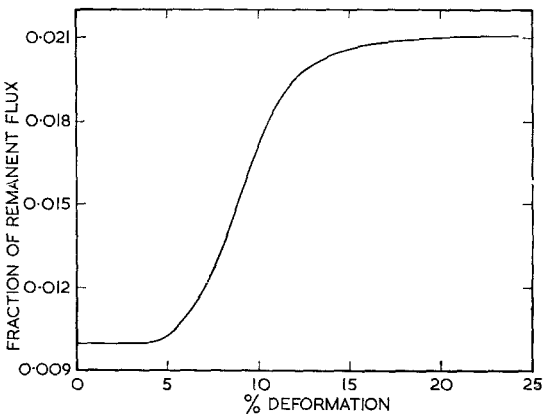

Figure 13 Remanent magnetisation expressed as a fraction of H_{c2} plotted versus percentage deformation.

would have occurred during the early stages of deformation, when most of the twins were created. This is not observed, suggesting that twin boundaries and their large internal strains are not as effective pinning centres for supercurrent vortices as are dislocation tangles. The grain-boundary structure remained practically unaltered during deformation, and it may be concluded that grain boundaries are also relatively weak barriers to flux movement in deformed specimens.

On comparing the curve of fig. 13 with the observed dislocation structure, it may be seen that for initial strains less than 4% there is very little increase in the remanent induction and dislocations are uniformly distributed. The cell formation begins at about 8% strain and is completed at 16% strain. During this stage the increase in remanent induction is most rapid. Once a non-uniform distribution is set up, further deformation makes only a relatively small contribution in enhancing the irreversibility; the dislocation distribution does not change, new dislocations are merely added to the cell walls making them thicker.

4.3. Heat-Treated Material

The magnetisation curves of specimens deformed 16% by rolling, followed by annealing for 1 h at 850, 950, 1050, and 1200° C are shown in fig. 14, and compared with that for the deformed but unannealed material. The annealing treatment increases the irreversibility; the higher the annealing temperature the greater the irreversibility. The results on the specimens annealed at the three lower temperatures is entirely consistent with the contention that an inhomogeneous distribution of dislocations is necessary to provide vortex pinning. Annealing increases this inhomogeneous dislocation distribution by the formation of polygonised cell boundaries. A similar result has been found on annealing Nb/Ta [14].

Annealing at temperatures above 1150° C causes precipitation of the non-superconducting sigma-phase. Normal particles are known to pin flux, and the increased irreversibility after high temperature annealing is quite expected. A detailed investigation into the effect of precipitation on the superconducting properties of this alloy is in progress, and will be reported later.

5. Comparison with Theory

In this section an attempt is made to relate quantitatively the results of magnetisation measurements with the flux-pinning model proposed by Campbell *et al* [11, 45]. The model has been found to be most satisfactory in predicting many irreversible magnetic properties of Pb/Bi alloys, where flux-pinning is mainly due to normal Bi particles.

For straight, parallel, flux lines, the critical state of an irreversible type II superconductor is given by [46]

$$\frac{\phi_0}{4\pi m}\frac{\mathrm{d}B}{\mathrm{d}x} = F_\mathrm{p} \qquad (6)$$

where F_p is the pinning force exerted by the microstructure acting per unit length of the flux line, ϕ_0 is a single quantum of magnetic flux (2×10^{-7} G cm^2) associated with each flux line, and m (≈ 1) is the slope of the reversible B-H curve. As the induction B increases so that the number of flux lines exceeds the number of pinning centres, it is expected that F_p should decrease [11, 45]. Considering the most general case where $F_\mathrm{p} = \mathrm{k}/B^n$ equation 6 becomes

$$F_\mathrm{p} = \frac{\mathrm{k}}{B^n} = \frac{\phi_0\,\alpha}{4\pi m\, 2B^n} \qquad (7)$$

where α is the pinning parameter given by $\alpha = 8\pi m\mathrm{k}/\phi_0$. Both α and n depend upon the microstructure, and their values for a particular specimen can be obtained from its magnetisation curve [47]. In the case of Pb/Bi alloys, a value of n equal to unity accounted for the observed magnetisation [11, 45, 48]. For the deformed Mo/Re specimens (fig. 12), however, the estimated value of n was 0.9.

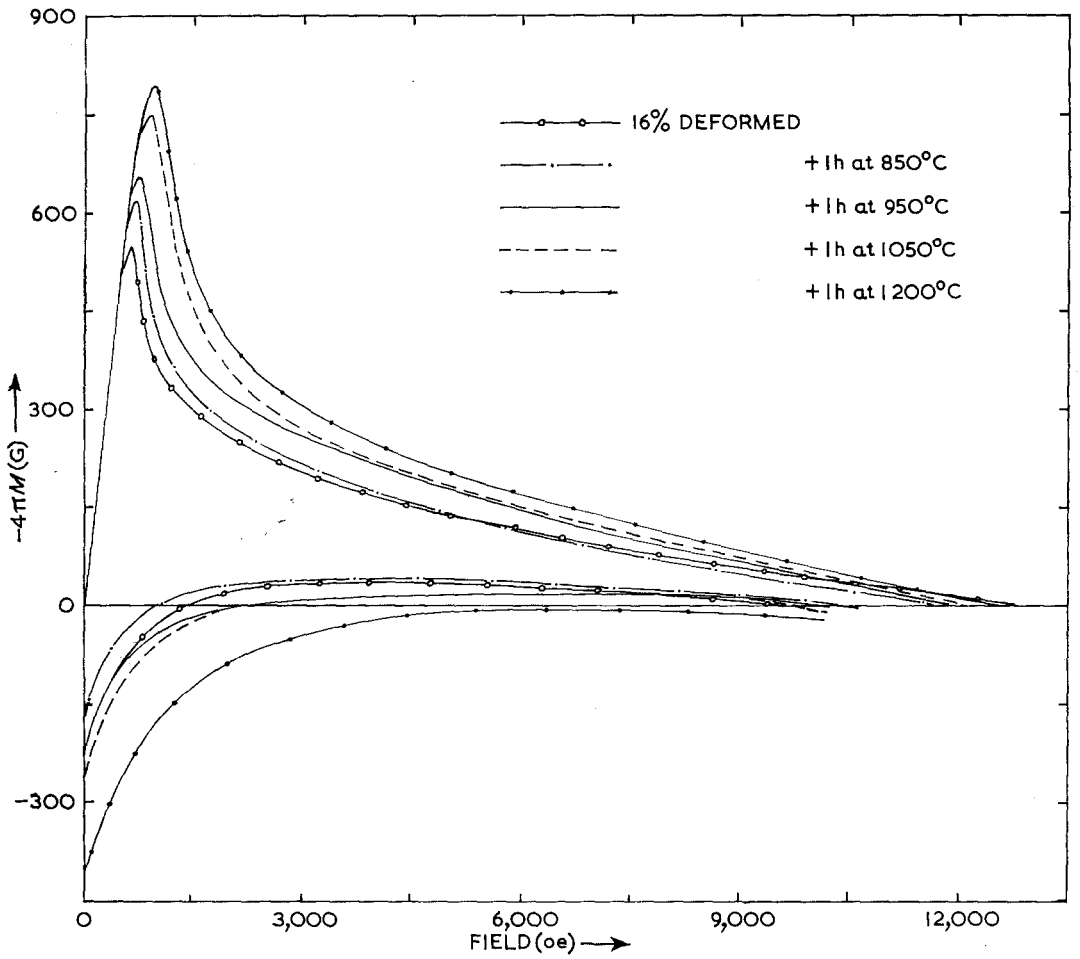

Figure 14 Magnetisation curves for annealed Mo/Re specimen. $+4\pi M$ values near H_{c_2} (H decreasing) for all the curves were very close to the H axis and they are omitted from the figure for the sake of clarity.

Following the procedure suggested by Campbell *et al* [11, 45] the analytical expressions for magnetisation for $n = 0.9$ are given by

(i) H_0 increasing; $H_{c_1} < H_0 < H_m$

$$-4\pi M = H_0 - \frac{1}{3.48\, a^2\alpha^2}\left[\{4.8\, B_0^{2.9}\, a\alpha - 2B_0^{4.8}\}\right. \quad (8)$$

(ii) H_0 increasing; $H_m < H_0 < H_{c_2}$

$$-4\pi M = H_0 - \frac{1}{3.48\, a^2\alpha^2}\{B_0^{2.9}[4.8\, a\alpha - 2B_0^{1.9}] + 2[B_0^{1.9} - 0.95\, a\alpha]^{\frac{4.8}{1.9}}\} \quad (9)$$

(iii) H_0 decreasing from H_{c_2} to H_{c_1};

$$-4\pi M = H_0 - \frac{1}{3.48\, a^2\alpha^2}\{2[B_0^{1.9} + 0.95\, a\alpha]^{\frac{4.8}{1.9}} - B_0^{2.9}[4.8\, a\alpha + 2B_0^{1.9}]\} \quad (10)$$

where H_0 is applied magnetic field, and H_m is the value of H_0 when the flux fronts meet at the centre of the specimen. B_0 is the magnetic induction at the surface in equilibrium with H_0 ($B_0 = H_0$ when $H_0 \gg H_{c_1}$), and a is the specimen radius.

Table IV gives the values of the pinning parameter α as obtained from the magnetisation curves of fig. 12. The magnetisation curves were most stable near $H_0 = 6$ kOe and these values of α were determined from the curves lying in this region.

Using equations 8, 9, and 10, and α from table IV, the calculated magnetisation curve of the 16% deformed specimen is compared with the experimental curve in fig. 15. The agreement between the two curves is reasonably good. Equations 8, 9, and 10 are derived for a long cylindrical specimen while the experimental

TABLE IV

Specimen	As-received	4% Deformed	8% Deformed	12% Deformed	16% Deformed	24% Deformed
Pinning constant α (kG$^{\frac{18}{10}}$/cm)	2.9	8.3	11.5	46.6	67.0	112.4
Pinning force F_p (dyn/cm) at $B = 5$kG as calculated using equation 7, values of α as above	—	—	—	9.3×10^{-5}	1.3×10^{-4}	2.2×10^{-4}
Pinning force F_p (dyn/cm) at $B = 5$kG exerted by dislocation cell walls as calculated using equation 11; d and L from table II	—	—	—	9.5×10^{-5}	4.0×10^{-4}	8.9×10^{-4}

curve was obtained for a flat strip. Compared to the calculated curve, the experimental curve has a smaller peak. This, presumably, is because of the occurrence of the flux jumps which are common near the peak magnetisation. The main disagreement between the two curves occurs near H_{c_2}, where the calculated magnetisation does not become zero. This is, however, a drawback of the model itself, as the theoretical pinning strength becomes zero only as $B \to \infty$, and not at H_{c_2}.

Using equation 7 with $n = 0.9$ and values of α from table IV the pinning force F_p at $B = 5$kG was calculated for deformed specimens. The values of F_p thus obtained for 12, 16, and 24% deformed specimens are given in table IV. The pinning force is enhanced by increasing amounts of deformation.

It has been suggested [14] that pinning by dislocation tangles should be essentially similar to that by normal particles. Since a normal particle has a different κ from the matrix there must be a circulating supercurrent at its surface. This supercurrent will interact with those of vortices to cause pinning. Dislocation tangles in a type II superconductor form regions of higher κ. The results in table III show that κ_1 is increased after deformation.

Campbell *et al* [11] have shown that if the microstructure consists of a distribution of normal particles, the pinning force F_p, at an induction B, exerted per unit length of the flux line is given by

$$F_p = \frac{4\pi M(\text{reversible})}{B^{\frac{1}{2}} L^3} \frac{d^2}{8\pi\lambda} \phi_0^{\frac{3}{2}} \qquad (11)$$

where L is the distance between the particles of diameter d, and λ is the penetration depth. For the Mo/Re alloy where pinning is believed to be mainly caused by dislocation cell walls, L should be taken as the distance between the cell walls, and d as their width.

For the Mo/Re alloy with $H_c = 1460$ Oe, and assuming $\kappa_{GL} = 5$, equation 1 gives $\lambda \approx 10^{-5}$ cm. Using this value of λ, and d and L from table II, the pinning force F_p exerted by dislocation cell walls was calculated from equation 11. The values of F_p thus obtained for 12, 16, and 24% deformed specimens are shown in table IV, and are found to agree reasonably well with those calculated from equation 7. This strengthens the contention that in the deformed alloy, the flux hindrance is mainly caused by dislocation tangles. To an order of magnitude, the values of F_p in table IV agree with the rough estimate obtained by Van Gurp and Van Ooijen by considering the electron mean free path in the tangles [49].

The agreement of the observed magnetisation with the theory of Campbell and Evetts is evident in fig. 15. The composite parameter $a\alpha$ (table IV) was expressed in units of k G$^{\frac{18}{10}}$. The agreement of the experimental results with the theory is further shown up when $(a\alpha)^{\frac{10}{19}}$ is plotted against percentage deformation; the curve obtained is very similar to the curve of fig. 13.

Although the experimental results described earlier suggest that both twin boundaries and grain boundaries are relatively ineffective in flux-pinning, there is a good reason to believe that their presence in the deformed specimens will influence the upper critical field. The observed increase in the normal state resistivity after deformation (4.2.) is too large to be explained by the increase in dislocation density alone (table II), and it is expected that the other defects such as point defects, grain boundaries, and twin boundaries will make some contribution to the resistivity [50, 51], and consequently they must also (equation 5) influence the upper critical field.

The reason why these defects are relatively ineffective in pinning flux lines must lie in their internal structure. Defects with a range of misfit in one dimension less than the range of coherence (~100 Å for this alloy) will not interact with vortices. This immediately rules out individual

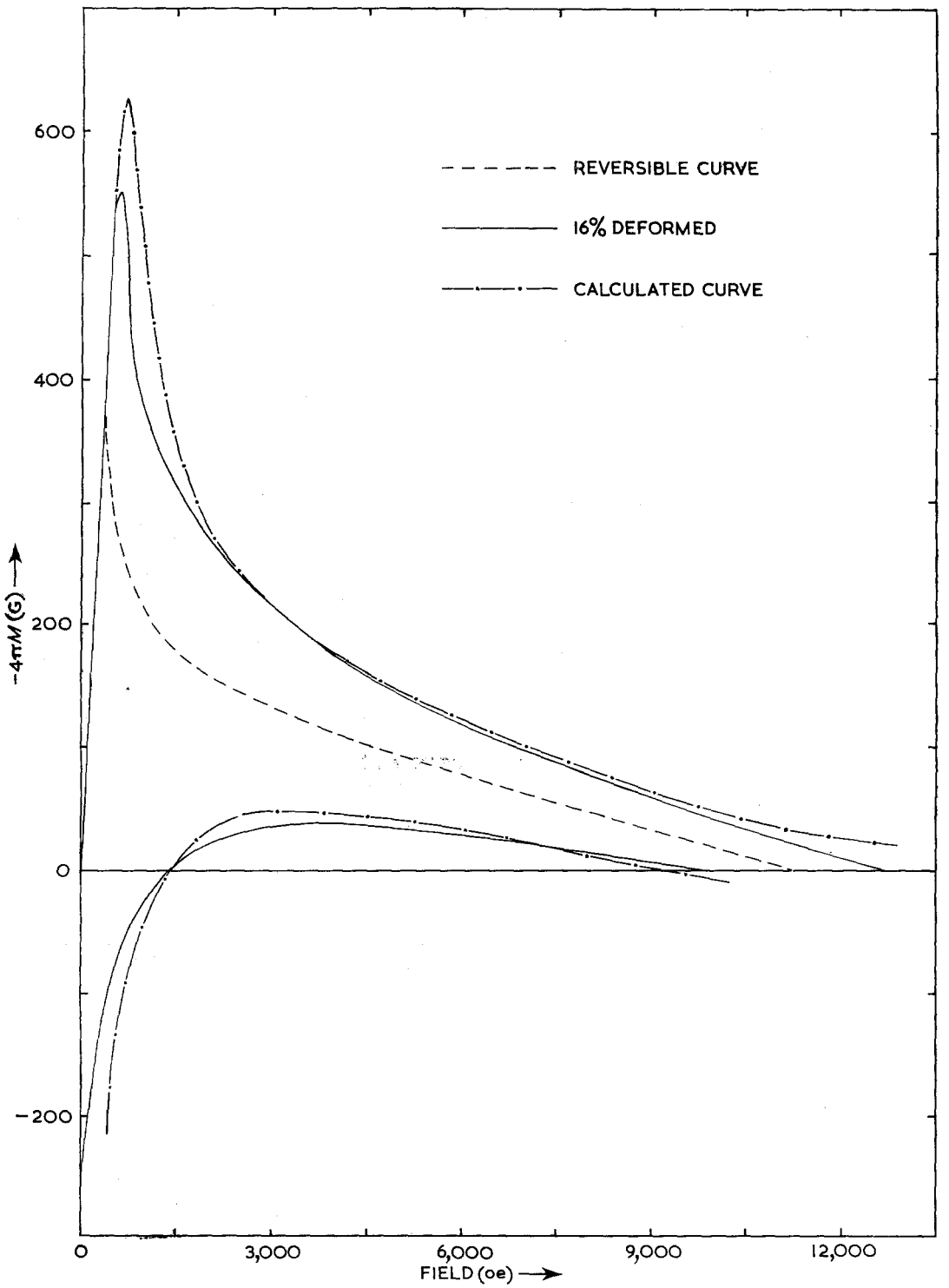

Figure 15 Calculated magnetisation curve compared with experimental magnetisation curve for 16% deformed specimen. $+4\pi M$ values near H_{c2} (H decreasing) for the experimental curve are not shown (see figs 12 and 14). Note that for the calculated curve, $-4\pi M$ does not become zero at H_{c2}. This feature is inherent in all the existing theoretical models of flux-pinning.

point defects as responsible for pinning. A grain boundary is now known to be [52] a layer of atomic misfit only two or three atoms wide and is consequently also too small to give rise to pinning. A non-coherent twin boundary is essentially similar to a grain boundary and will also fail to produce pinning.

Acknowledgements

This work was financially supported by the Science Research Council. The authors would like to thank Mr J. D. Llewellyn and Mr D. J. Brassington for their experimental help, and Mr D. Ward for fruitful discussions. They are grateful to Professor E. R. Dobbs and the Physics Department at Lancaster for the provision of facilities to pursue this work. One of us (M.J.W.) wishes to thank the Science Research Council for the award of an Advanced Course Studentship.

References

1. J. K. HULM, *Phys. Rev.* **98** (1955) 1539.
2. R. D. BLAUGHER, A. TAYLOR, and J. K. HULM, *IBM J. Res. Development* **6** (1962) 116.
3. J. E. KUNZLER, E. BUEHLER, F. S. L. HSU, B. T. MATHIAS, and C. WAHL, *J. Appl. Phys.* **32** (1961) 325.
4. E. LERNER and J. G. DAUNT, *Phys. Rev.* **142** (1966) 251.
5. E. LERNER, J. G. DAUNT, and E. MAXWELL, *ibid* **153** (1967), 487.
6. C. T. SIMS, *Trans. Amer. Soc. Metals*, **51** (1959), 1068.
7. J. M. DICKINSON and L. S. RICHARDSON, *ibid* p. 1055.
8. A. LAWLEY and R. MADDIN, *Trans. AIME* **224** (1962) 573.
9. K. OGAWA and R. MADDIN, *Acta Met.* **12** (1964) 1161.
10. J. D. LIVINGSTON, *Phys. Rev.* **129** (1963) 1943.
11. A. M. CAMPBELL, J. E. EVETTS, and D. DEW-HUGHES, to be published.
12. J. J. HAUSER and E. BUEHLER, *Phys. Rev.* **125** (1962) 142.
13. J. J. HAUSER and E. HELFAND, *ibid* **127** (1962) 386.
14. A. V. NARLIKAR and D. DEW-HUGHES, *J. Matls. Sci.* **1** (1966) 317.
15. E. VOTAVA, *Acta Met.* **10** (1962) 745.
16. E. VOTAVA and A. W. SLEESWYK, *ibid* p. 965.
17. K. OGAWA and R. MADDIN, *ibid* **12** (1964) 713.
18. D. HULL, Proc. 5th International Conf. on Electron Microscopy (Philadelphia, 1962).
19. C. N. REID, *J. Less Common Metals* **9** (1965) 105.
20. J. D. LIVINGSTON and H. W. SCHADLER, *Progr. Matls. Sci.* **12** (1965) 183.
21. J. A. CATTERALL, *Met. Rev.* **11** (1966) 25.
22. D. DEW-HUGHES, *Mat. Sci. Eng.* **1** (1966) 2.
23. B. B. GOODMAN, *Reports Progr. Phys.* **29** (1966) 445.
24. A. A. ABRIKOSOV, *JETP* **32** (1957) 1442.
25. J. L. HARDEN and V. ARP, *Cryogenics* **3** (1963) 105; L. NEUMANN and L. TEWORDT, *Z. Physik* **189** (1966) 55.
26. K. MAKI, *Physics* **1** (1964) 21, 127; *Phys. Rev.* **148** (1966) 362.
27. L. P. GOR'KOV, *JETP* **37** (1959) 803, 1407.
28. C. CAROLI, M. CYROT, and P. G. DEGENNES, *Solid State Commun.* **4** (1966) 17.
29. C. N. REID, A. GILBERT, and G. T. HAHN, *AIME* Conf. on Deformation Twinning (Florida, 1963) (Gordon and Breach, New York, 1965).
30. G. W. GEIL and N. L. CARWILE, *Trans. AIME* **197** (1953) 213.
31. D. HULL, AIME Conf. on Fracture of Solids (Interscience, New York, 1962).
32. A. W. SLEESWYK and C. A. VERBRAAK, *Acta Met.* **9** (1961) 917.
33. A. W. SLEESWYK, *ibid* **10** (1962) 705.
34. D. HULL, *ibid* **9** (1961) 909.
35. J. WASHBURN, G. W. GROVES, A. KELLY, and G. K. WILLIAMSON, *Phil. Mag.* **5** (1960) 991.
36. R. K. HAM, *ibid* **6** (1961) 1183.
37. A. G. KNAPTON, *Trans. Amer. Soc. Metals* **51** (1959) 1067.
38. B. BERTMAN, D. G. SCHWEITZER, and F. P. LIPSCHULTZ, *Phys. Letters* **21** (1966) 260.
39. A. ECHARRI, Dr. Spec. Phys. Thesis, Grenoble (1965).
40. *Idem, Phys. Letters*, **20** (1966) 619.
41. F. J. MORIN and J. P. MAITA, *Phys. Rev.* **129** (1963) 1115.
42. B. MUHLSCHLEGEL, *Z. Physik* **155** (1959) 313.
43. C. J. GORTER and H. B. G. CASIMIR, *Physica* **1** (1934) 306.
44. B. B. GOODMAN, *IBM J. Res. and Development* **6** (1962) 63.
45. A. M. CAMPBELL, J. E. EVETTS, and D. DEW-HUGHES, *Phil. Mag.* **10** (1964) 333.
46. J. FRIEDEL, P. G. DE GENNES, and J. MATRICON, *Appl. Phys. Letters* **2** (1963) 119.
47. J. E. EVETTS, A. M. CAMPBELL, and D. DEW-HUGHES, to be published.
48. *Idem, Phys. Letters* **16** (1965) 113.
49. G. J. VAN GURP and D. J. VAN OOIJEN, *J. Physique* **27** (1966) C3-51.
50. H. M. ROSENBERG, "Low Temperature Solid State Physics" (Oxford University Press, Oxford, 1963).
51. V. F. FORSTER and E. SCHELL, *Z. Metallk.* **32** (1940) 165.
52. D. G. BRANDON and M. WALD, *Phil. Mag.* **6** (1961) 1035.
53. J. J. HAUSER and R. G. TREUTING, *J. Phys. Chem. Solids* **24** (1963) 371.
54. M. S. WALKER and M. J. FRASER, Scientific Paper 62-125-280-PI (Westinghouse Research Laboratories, 1962).
55. M. S. WALKER, R. STICKLER and F. E. WERNER, Scientific Paper 62-141-448-P2 (Westinghouse Research Laboratories, 1962).
56. J. D. EMBURY, *Trans. Met. Soc. AIME* **236** (1966) 1252.